Gold metallization of hybrid organic-inorganic polymer microstructures 3D printed by two-photon polymerization

Kateryna Bretosh, Simon Hallais, Clotaire Chevalier-Cesar, Gaël Zucchi, Laurence Bodelot

Gold metallization of hybrid organic-inorganic polymer microstructures 3D printed by two-photon polymerization

Kateryna Bretosh[1], Simon Hallais[1], Clotaire Chevalier-Cesar[1], Gaël Zucchi[2], Laurence Bodelot[1,*]

[1] LMS, CNRS, École Polytechnique, Institut Polytechnique de Paris, Route de Saclay, 91128 Palaiseau Cedex, France

[2] LPICM, CNRS, École Polytechnique, Institut Polytechnique de Paris, Route de Saclay, 91128 Palaiseau Cedex, France

*Corresponding author: laurence.bodelot@polytechnique.edu

Highlights

- A strategy was established to coat printed hybrid polymer microstructures with gold
- The influence of procedure parameters on the gold layer quality were investigated
- The morphology, thickness and conductivity of the gold layers were characterized
- Electrical resistivities lower than twice that of bulk gold can be reached
- This conformal method can be used to coat micrometric structures of arbitrary shapes

Abstract

Two-photon polymerization is a femtosecond laser-based technique enabling printing of three-dimensional structures down to submicron resolution within photocurable polymers. Rendering the dielectric 3D printed structures conductive can be of great interest for various applications in domains such as energy, photonics, or multifunctional devices. In this work, the microstructures of interest are made of a silicon-zirconium hybrid organic-inorganic polymer exhibiting low shrinkage during development. A simple and efficient metallization method by electroless plating

is investigated to deposit a gold layer on the surface of the printed microstructures. The influence of the method parameters on the quality and properties of the deposited layer is studied. Among these parameters, the surface modification agent concentration and step duration, as well as the seeding solution concentration, must be adapted to the specific case of the considered hybrid microstructures. The concentration of metal ions in the plating bath is the most influential parameter on the morphology of the deposited gold layers. In particular, higher concentrations lead to smooth and continuous layers with electrical conductivities lower than twice that of bulk gold. Finally, the deposited layers are shown to coat 3D printed microstructures of arbitrary shapes, thus confirming the conformality of the method at the micrometric scale.

Keywords

Metallic coating, electroless plating, 3D printing, two-photon polymerization, hybrid organic-inorganic polymer, electrical conductivity

1. Introduction

Macroscopic-scale 3D printing is now ubiquitous for a wide variety of materials including thermoplastics, polymers, ceramics, metals, concrete, composites, and biomaterials [1]. In contrast, 3D printing with a resolution down to the submicron scale has remained limited to direct laser writing (DLW), and more particularly to two-photon polymerization (TPP) of photocurable polymers by femtosecond lasers [2–4]. The fabricated nano/micro-structures have applications mainly in optics [5–7], micromechanical systems [8,9], biocompatible scaffolds [10–12], microrobotics [13], and anticounterfeiting [14]. Leveraging the possible photoreduction of certain metallic ions concomitant to the TPP process, metal-salt-based photoresists have been proposed to obtain conductive metallic nano/micro-structures [15–17]. However, such resists do not permit a

truly three-dimensional structuration. Hence rendering conductive at least the surface of 3D dielectric nano/micro-structures is of great interest to extend the breadth of potential applications of these structures to multifunctional devices [18], especially in the fields of flexible electronics [19], photonics [20] or catalysis [21].

Several methods exist to coat dielectric polymers with a metal layer and thus to endow them with properties that are usually associated with metals, such as reflectivity, magnetic properties or electrical conductivity [22]. These methods, known as electroless methods, can be carried out either in gaseous or liquid phases (see Fig. 1). Nevertheless, covering three-dimensional structures with a conformal metal coating is not straightforward. Physical vapor deposition (PVD) methods are restricted to planar surfaces since they possess directional deposition effects [23]. In general, chemical vapor deposition (CVD) techniques are not conformal on the surface of complex geometries because of the limited mass diffusion that leads to a difference of deposition rate on the inner and outer surfaces of the structure. In fact, among CVD techniques, only atomic layer deposition (ALD) is known for its high quality, 3D conformality and smooth surface coating [24]. However, ALD possesses several drawbacks such as a limited number of vaporizable precursors, a long duration to grow a thick film as well as a high precursor gas energy usage (about 60% of the precursor is wasted) and high energy consumption. In comparison, electroless plating offers overwhelming advantages: conformality on complex geometries, mild conditions (generally, at room temperature and in aqueous media), simple reaction procedure (no special reactor required) that can even be conducted in a microfluidics environment [25], and low cost (surface catalyst and electroless plating bath only needed) [26].

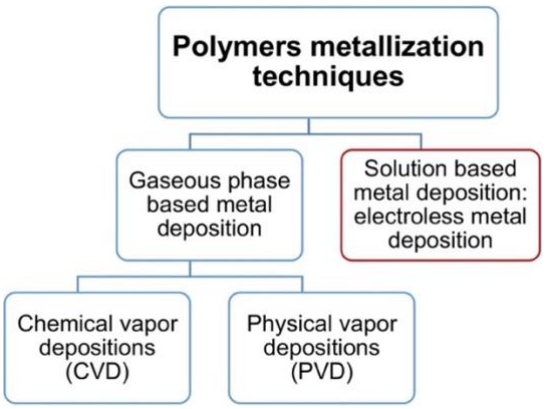

Fig. 1. Schematic of polymer metallization techniques.

More particularly, electroless plating is a chemical reduction of metal ions in an aqueous medium containing a reducing agent. Contrary to other techniques, where metal deposition directly follows surface conditioning, electroless plating consists of three main steps: 1) surface modification, 2) surface activation, or seeding, with a catalyst, and 3) plating, that is the chemical deposition onto the seeded substrate of a metal film from a solution (the electroless plating bath) containing a reducing agent and a metal derivative. In principle, it is possible to deposit any metal on a polymer substrate as long as an appropriate catalyst is used to activate the surface. Table S1 (see Section 1 of the Supplementary Material) lists a variety of polymeric surfaces that can be metallized using the electroless plating technique (here, with the most widely used metals, i.e., Ni, Cu, Ag, Au) with different surface activation methods. Because of its higher cost, gold plating is not as developed as nickel and copper plating, but it remains very important, as a noble metal, to prepare uniform patterns for microelectronics [27], fuel-cells [28], or surface-enhanced sensing [29,30].

Among photocurable polymers, acrylate-based polymers were the first polymers used for TPP [2], and they remain the most widely used because of their extremely photoactive and chemically tunable structure. Among them, Ormocomp, that belongs to the organically modified ceramics (ORMOCER) family, has a good chelating ability to silver ions, which is very important for

activating the surface before Cu electroless plating. Hence, electroless Cu plating of Ormocomp 3D printed structures was reported to yield a uniform deposition of thick and continuous copper coatings [19]. Other TPP polymers based on the combination of methacryloxypropyl trimethoxysilane (MAPTMS), zirconium propoxide (ZPO), and 2-(dimethylamino)ethyl methacrylate (DMAEMA) were also successfully plated with silver [31,32]. Since NH_2 groups of DMAEMA are especially active, they facilitate the coordination of metal ions and allow the growth of the metal layer on the surface of the polymeric structures. To the best of our knowledge, Au electroless plating of 3D structures printed by TPP has only been reported on structures made of pentaerythritol triacrylate (PETA) [21]. In this case, the Au electroless plating protocol was performed using an acid treatment followed by seeding with an Au-dimethylaminopyridine (Au-DMAP) complex and, finally, by plating in an Au-NH_2OH bath. This simple, three-step electroless procedure showed high efficiency on acrylate-based polymers, and a uniform, somewhat conductive, gold foam was obtained after removing the polymer by baking.

In this work, the polymer of interest for 3D printing via TPP is a hybrid silicon-zirconium organic-inorganic photosensitive material (SZ2080) that is known for its excellent optical properties, its good mechanical and chemical stability, as well as its very low shrinkage during development [33]. Compared to the resins plated in [31,32], it contains MATPMS and ZPO but no DMAEMA and, thus far, electroless plating of structures printed out of pure SZ2080 has not been reported. However, since PETA and SZ2080 both have active methacrylic groups, the principles of the metallization method proposed by Kim *et al.* [21] for acrylate plastics are revisited and successfully adapted to SZ2080 printed structures. Thereby, a simple and efficient method is devised to cover the non-conductive surfaces of 3D printed SZ2080 hybrid organic-inorganic polymer microstructures with highly conductive gold layers via electroless plating. The influence

of different experimental parameters on the quality and properties of the deposited gold layer are investigated and reported in this work.

2. Experimental

2.1. Materials

The chemicals used to perform electroless plating in this work were purchased from Sigma-Aldrich and VWR and were used without further purification. The list of products, along with their CAS number in parenthesis, is the following: gold(III) chloride trihydrate (27988-77-8), tetraoctylammonium bromide (14866-33-2), 4-dimethylaminopyridine (1122-58-3), sodium borohydride (16940-66-2), hydroxylamine hydrochloride (540-11-01), hydrochloric acid (7647-01-0) and toluene (108-88-3).

2.2. 3D printing

The polymer, SZ2080, is a sol-gel organic-inorganic hybrid composite containing silicon and zirconium in a 4 to 1 molar ratio. It was synthesized by adding a mixture of methacrylic acid and zirconium propoxide (ZPO, 70% in propanol) to hydrolyzed methacryloxypropyl trimethoxysilane (MAPTMS) according to the method reported in [33], with the addition of 1 wt% of 4,4'-Bis-(diethylamino)-benzophenone (IRG369) as the photoinitiator. Before printing, a drop of the material was casted onto a glass slide and heated up to 90°C for 20 min. The laser used for TPP in this work is a Pharos Yb:KGW laser operating at 515 nm with a 271 fs pulse duration, a repetition rate of 1 MHz and a power of 0.5 mW. All structures were printed using a 20x NA0.8 objective (Plan-Apochromat from Zeiss), a hatching (horizontal step) of 0.4 µm as well as a slicing (vertical step) of 0.6 µm for the parallelepided and of 0.5 µm for the other two structures (see below). After printing, the structures were developed in isobutyl methyl ketone for 45 min to remove the uncured

material.

The structure used to study the influence of the electroless plating parameters is a parallelepiped of dimensions 400 µm x 200 µm x 80 µm with 55 µm diameter through holes (see Fig. 2). The other structures used to demonstrate the conformality of the coating (see Section 3.8) are two adjacent cubic cells with inner diagonals of overall dimensions 220 µm x 120 µm x 120 µm with 20 µm diameter bars as well as a tetrahedron of overall dimensions 110 µm x 95 µm x 90 µm with 5 µm diameter bars. With the reported writing parameters, the printing times are ~22 min for the parallelepiped, ~8 min for the cubic cells, and ~30 s for the tetrahedron.

2.3. Electroless plating procedure

The Au electroless plating procedure was adapted from the one proposed by Kim *et al.* [21] in the context of polyacrylate plastics plating. It consists of three main steps and allows depositing a gold layer on the surface of the insulating 3D printed SZ2080 structures (see Fig. 2). It includes: 1) surface modification with hydrochloric acid (HCl), 2) seeding with 4-dimethylaminopyridine-stabilized gold nanoparticles (Au-DMAP), and 3) gold plating in a bath made of gold(III) chloride trihydrate ($HAuCl_4 \bullet 3H_2O$) dissolved in an hydroxylamine hydrochloride ($NH_2OH \bullet HCl$) aqueous solution. Firstly, the HCl treatment provokes the ester hydrolysis of SZ2080 and leads to the formation of $–COO^-$ groups on the surface of the printed structure (the pKa of acrylic acid is between 4 and 5, which means that, in a neutral medium, it mostly exists in the form of its conjugate base COO^-). The negative charge of carboxylates on the surface of the structure then facilitates the attraction of the positively charged Au-DMAP nanoparticles that play a catalytic role for the further gold layer deposition using hydroxylamine as a reductant.

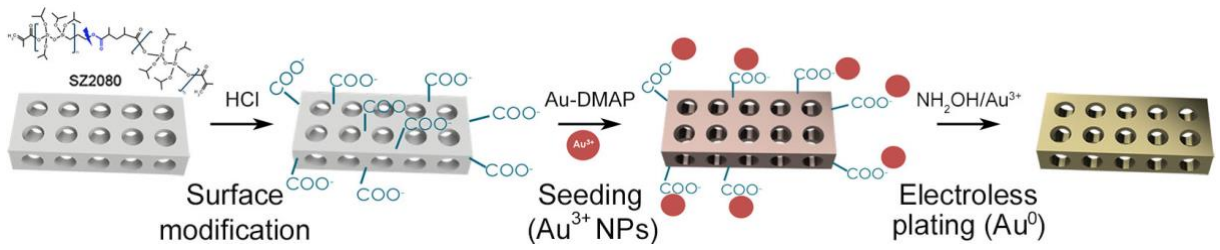

Fig. 2. Schematic illustration of Au electroless plating of SZ2080 3D printed structures.

In the surface modification step, a SZ2080 3D structure printed on a glass slide was first immersed in an aqueous solution of HCl (18.5 wt%) for 2 h. Then, the glass slide with the printed structure was rinsed, dipped in deionized (DI) water for 5 h, and dried under N_2 flow.

For conducting the seeding step, the COO^- modified structure (attached to the glass slide) was immersed in the suspension of Au-DMAP nanoparticles for 15 h. Then, the seeded structure was removed, dipped in DI water for 5 h, and dried under N_2 flow. Details on the Au-DMAP solution used in this step are given in Section 2 of the Supplementary Material. In particular, in the case of micrometric structures printed on a glass slide, the as-synthesized solution was so dense that the solution front was peeling the 3D printed structures off their glass slides upon either insertion or removal of the slides in or out of the solution. Hence, the initial nanoparticle solution was systematically further diluted 4.25 times before use in the plating procedure in order to reduce the nanoparticle concentration, and thus the surface tension.

Concerning the electroless Au plating step, the seeded structure (attached to the glass slide) was immersed in an aqueous solution of NH_2OH•HCl and $HAuCl_4$•$3H_2O$ with respective concentrations of 0.92 M and **2×10^{-2} M**, and the molar ratio between NH_2OH•HCl and $HAuCl_4$•$3H_2O$ kept constant for other $HAuCl_4$•$3H_2O$ concentrations. The structure was left in the plating bath for **5 min**. Afterwards, the gold-coated structure was dipped in DI water for 2 h, and dried under N_2 flow.

Note that the information indicated in bold in the three steps described above corresponds to the final values that were retained for the procedure tailored to the specific case of SZ2080 Au electroless plating. Such a procedure yielded a coating demonstrating both conductivity as well as a smooth and continuous layer morphology. Indeed, in this work, the influence of four main parameters impacting the quality and properties of the deposited gold layer was studied in detail. These parameters are:

- Concentration of HCl in the surface modification step
- Duration of the surface modification step
- Duration of the electroless plating step
- Concentration of $HAuCl_4 \bullet 3H_2O$ in the electroless plating step

2.4. Characterizations

The plated structures were observed with an FEI Quanta 600 FEG scanning electron microscope (SEM) at an operating acceleration voltage of 15 keV in low vacuum mode (10 Pa), and with an angular backscattered (ABS) detector in order to obtain images with contrasts based on the difference in atomic numbers of the elements interacting with the electron beam. In the specific case of the gold-plated polymer structures, interaction with the gold yields a very light contrast whereas interaction with the polymer yields a very dark contrast, which is convenient to evaluate the uniformity of the gold layer deposited on the structure.

Energy dispersive X-ray (EDX) spectroscopy analyses were performed at 5.22 nA with an acceleration voltage of 8 keV within the above-mentioned SEM with a PentaFET Precision 10 mm^2 X-act series detector from Oxford Instruments to determine the chemical composition of the plated layers.

The roughness and thickness of the gold layers were measured using a Bruker Dimension Icon atomic force microscope (AFM) with ScanAsyst. For roughness measurements, images were acquired in peak force tapping mode on a 10 µm x 10 µm field of view with a pixel size of 5 nm. S_a (arithmetical mean height) and S_q (root mean square height) of the probed surface were then calculated after performing a first order plane fit leveling of the data. For the thickness measurements, images were also acquired in peak force tapping mode but on a larger surface where the layer exhibited a scratch uncovering the polymer substrate, and with a pixel size of 30 nm. The thickness was then measured as the difference between the average height of the gold layer and that of the polymer surface after performing a first order plane fit leveling of the data.

Finally, the electrical properties of the gold layers were measured with a collinear four-point probe system equipped with a Keithley 4200-SCS. A current I of 0.1 A was applied between the outer probes and the electrical potential difference ΔV (in V) was measured between the inner probes. The resistivity $\rho\ (\Omega.m)$ of the gold layer was then obtained via the relationship $\rho = \pi/\ln(2)\,.\,C\,\frac{\Delta V}{I}\,.\,t$, with C a geometric factor (depending on the probes interspace and layer in-plane dimensions), and t the layer thickness [34].

3. Results and discussion

3.1. Influence of HCl concentration and of HCl treatment duration

Kim *et al.* [21] have reported a procedure to deposit a gold coating on polyacrylates using electroless plating. Particularly, a concentrated aqueous solution of 37 wt% HCl was used for one to two days in the surface modification step. In the case of SZ2080 microstructures, which are much smaller, such an HCl treatment leads to the disappearance of the printed structures from the glass slide possibly due to their dissolution or detachment from the slide. Thus, an adapted

procedure had to be developed to yield a gold coating of good quality without degrading nor losing the SZ2080 3D printed structures.

To determine both suitable HCl concentration and treatment duration in the surface modification step of the SZ2080 structures, a starting HCl concentration of 3.7 wt% was first employed with a treatment duration of 5 h. The acid concentration was then increased to 11.1, 18.5 and 25.9 wt%. In all cases, the intermediate washing steps were fixed at 5 h, the Au-DMAP treatment step at 15 h, the gold plating step at 30 min with an $HAuCl_4 \cdot 3H_2O$ concentration of 0.5×10^{-2} M, and the final washing step at 2 h. Backscattered electron (BSE) SEM images of the corresponding plated structures are reported in Fig. 3. Note that all images correspond to top views of the 3D printed structures, so that the observed surfaces are entirely in focus.

With the 3.7 wt% and 11.1 wt% HCl concentrations (Fig. 3a, c), the overall gold layer covering the structure exhibits non uniformities. Indeed, some areas appear with a darker contrast on the SEM images (1st inter-hole at the bottom left in Fig. 3a and 3rd inter-hole at the bottom in Fig. 3c). These darker areas indicate that the primary contribution to the collected signal comes from the polymer that is underneath the gold layer, thereby revealing that the gold layer is much thinner at these specific locations. For an HCl concentration of 18.5 wt% (Fig. 3e), the gold coating appears more uniform in contrasts at the surface of the structure. Beyond this concentration, and notably after a 25.9 wt% HCl treatment, the SZ2080 structure can no longer be found on the glass slide where it was printed. This is an indication that either dissolution or detachment from the glass substrate occurred.

For all HCl concentrations presented in Fig. 3, aggregates can be observed on the surface of the plated structures. These aggregates, in the form of bundled flakes, are constituted of gold since they appear as the whitest elements in the SEM images (see, for instance, Fig. 3d). After removal of the samples from the plating bath, gold always sediments at the bottom of the beaker. It is thus assumed that some of Au^{3+} NPs deposited on the structure in the seeding step detach from it and disperse in the plating bath. As a result, some gold flakes nucleate in the plating bath away from the structure. Some of them migrate towards the structure whereas others remain in the bath and eventually sediment. As will be seen in Section 3.3, aggregates become less predominant and visible at higher gold concentrations.

Additionally, SEM images of the coatings at higher magnification (Fig. 3b, d, f) show that the morphology of the gold layers evolves with HCl concentration. For a 3.7 wt% HCl concentration (Fig. 3b), the gold layer is barely formed on the surface of the polymer since one can only observe islands of lighter contrasts (gold) surrounded by large amounts of darker contrasts (uncovered polymer), akin to a mud-crack pattern. As the HCl concentration increases to 11.1 wt% (Fig. 3d), the dark crack-like network is less widespread and the lighter contrast areas start densifying. For an 18.5 wt% HCl concentration, areas of light contrasts further densify, and the dark crack-like

network no longer dominates the morphology. It is the densest layer obtained without losing the printed structure as well as the most uniform layer at the scale of the plated structure.

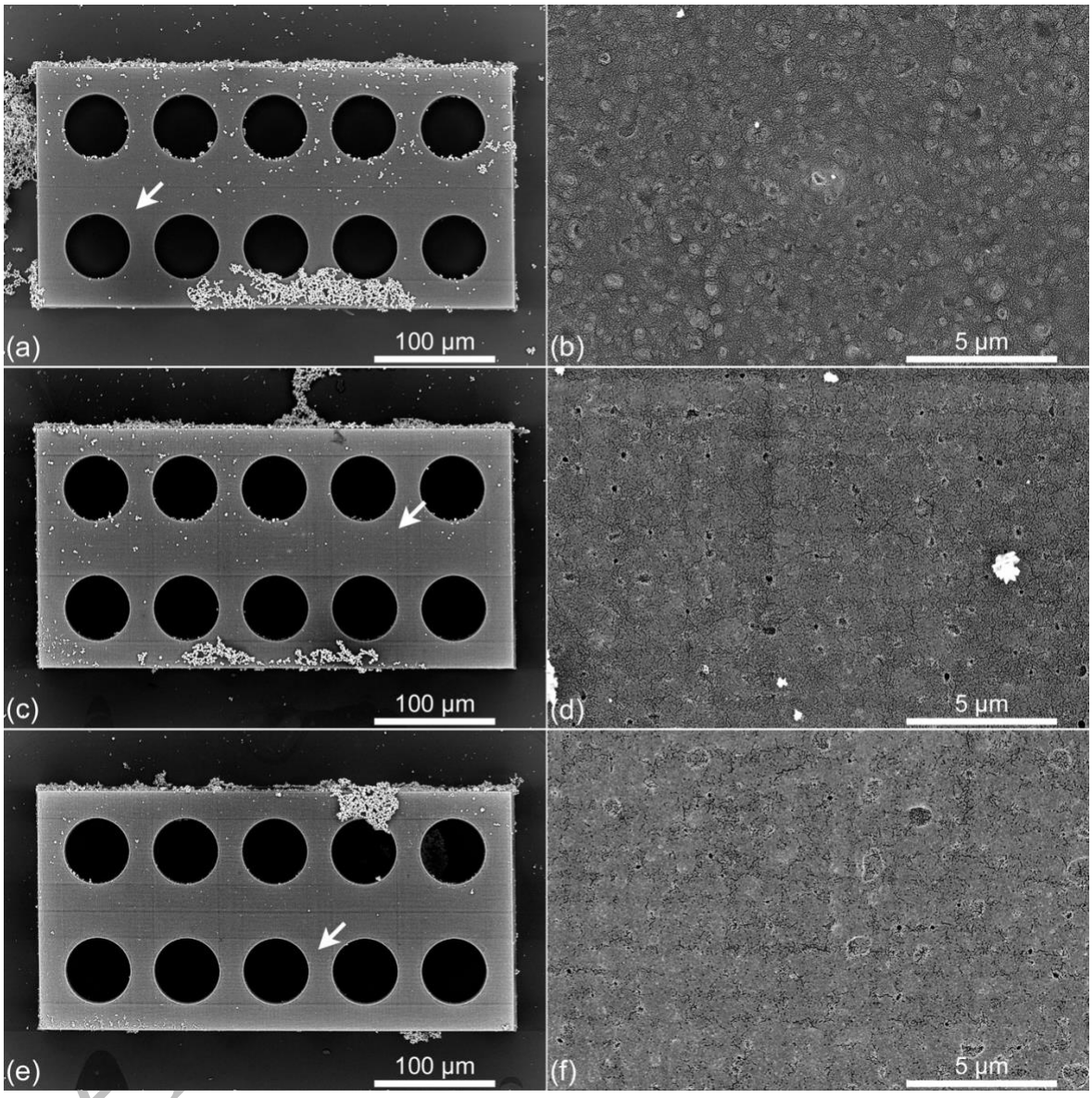

Fig. 3. Backscattered electron (BSE) SEM images of the coated SZ2080 microstructures and of the corresponding gold layers for a treatment duration of 5 h with an HCl solution of concentration (a, b) 3.7 wt%, (c, d) 11.1 wt% and (e, f) 18.5 wt%. The intermediate washing steps were fixed at 5 h, the Au-DMAP treatment step at 15 h, the gold plating step at 30 min with an $HAuCl_4 \bullet 3H_2O$ concentration of 0.5×10^{-2} M, and the final washing step at 2 h. The arrows in the left panels indicate the centers of the areas where the zooms of the right panels were taken.

Next, the duration of the HCl treatment step was varied to elucidate whether concentration or duration is predominant in this step. Since a 5 h treatment at 3.7 wt% appears insufficient to form a dense layer, the duration of the treatment was increased to 24 h. As reported in Section 3 of the Supplementary Material and in Fig. S2, increasing the duration of the 3.7 wt% HCl treatment step from 5 h to 24 h has no impact on the overall uniformity nor on the local morphology of the formed gold layer. Shorter treatment times were also tested for the highest HCl concentration that did not cause any degradation of the structure (i.e., 18.5 wt%). A 1 h treatment duration leads to a slightly less uniform overall coating (see the darker zone around the 3rd inter-hole at the top of the structure in Fig. 4a), whereas a 2 h treatment duration (Fig. 4c) appears to yield a coating with an overall uniformity similar to that obtained for a 5 h treatment duration (Fig. 3e). At a higher resolution, the layer obtained in the 1 h treatment (Fig. 4b) actually exhibits a much more widespread dark crack-like network. Conversely, the 2 h and 5 h treatments (Fig. 4d and Fig. 3f, respectively) both yield a much denser gold layer having the least amount of non-covered polymer, with the latter layer being only marginally denser than the former.

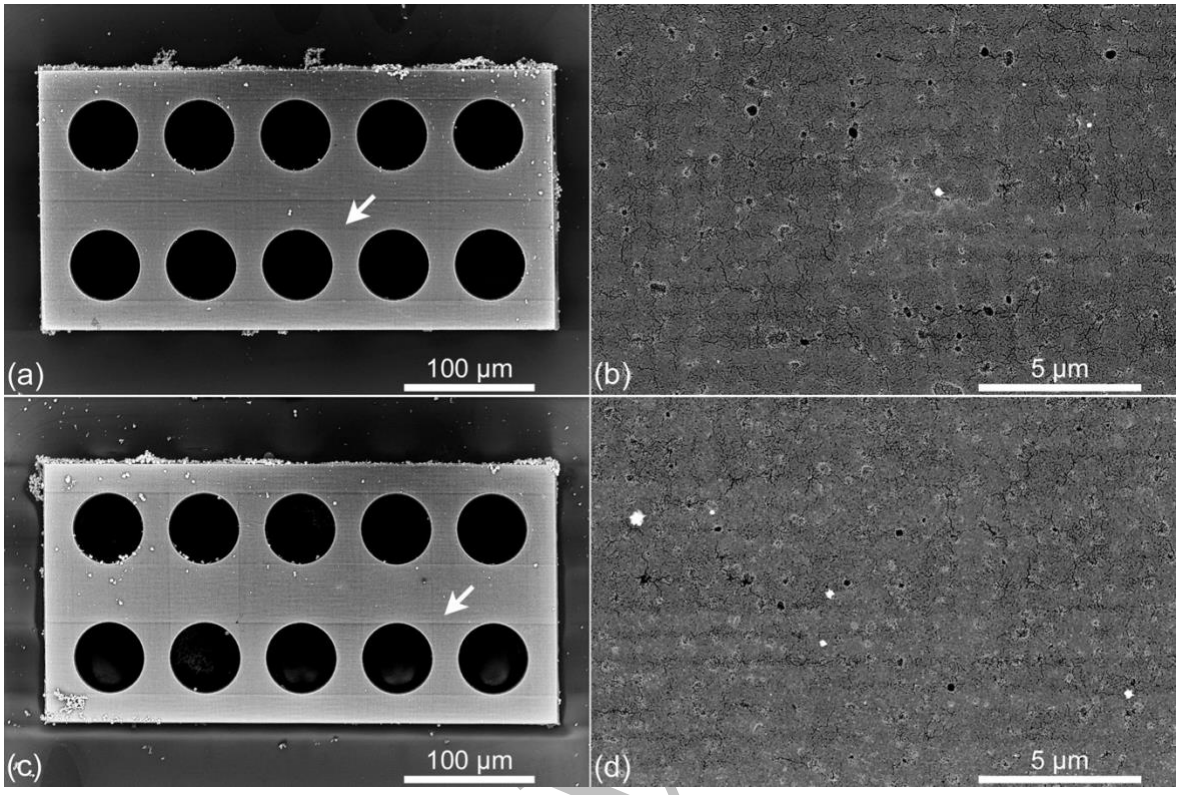

Fig. 4. BSE SEM images of the coated SZ2080 microstructures and of the corresponding gold layers for a treatment with an HCl solution of concentration 18.5 wt% for a duration of (a, b) 1 h and (c, d) 2 h. The intermediate washing steps were fixed at 5 h, the Au-DMAP treatment step at 15 h, the gold plating step at 30 min with an $HAuCl_4 \cdot 3H_2O$ concentration of 0.5×10^{-2} M, and the final washing step at 2 h. The arrows in the left panels indicate the centers of the areas where the zooms of the right panels were taken.

Hence, increasing the HCl concentration has a much more pronounced effect than increasing the treatment duration at lower HCl concentration. In particular, in the case of SZ2080 structures, the highest concentration of HCl that can be used without damaging the structures is 18.5 wt%. Such a treatment increases locally the surface roughness of the polymer via nano-pitting (see Section 4 of the Supplementary Material), thereby creating preferential sites for the attachment of nanoparticles in the next step of the electroless plating procedure (i.e., surface activation or seeding) as also reported after H_2SO_4 treatment of acrylate-based polymers [35].

In conclusion, the gold layer is found to be the most uniform and dense in only two cases: 18.5 wt% HCl for 2 h and 18.5 wt% HCl for 5 h. Even though the layer obtained in case of the 5 h treatment is marginally denser, in the interest of accelerating the procedure, a 2 h treatment with an 18.5 wt% HCl solution was finally retained for further investigation of the other parameters.

3.2. Influence of the plating step duration

After defining the optimal parameters for the surface modification step, the influence of the electroless plating step duration on the coating quality was studied. Note that the seeding step parameters (solution concentration and step duration) were not further investigated. Indeed, the highest possible concentration of the Au-DMAP solution was selected but dictated by surface tension considerations (see Section 2.3, and Section 2 of the Supplementary Material). The longest time was also selected while favoring the shortest overall procedure, and it corresponds here to an overnight step (15 h). Herein, the plating time was decreased with a fixed concentration of $HAuCl_4 \bullet 3H_2O$ of 0.5×10^{-2} M and SEM images corresponding to plating times of 20, 10 and 5 min are reported in Fig. 5.

By comparing Fig. 4c (30 min) to Fig. 5a, c, e (20 min, 10 min, 5 min, respectively), it appears that for the considered $HAuCl_4 \bullet 3H_2O$ concentration, the plating step duration has no impact on the overall uniformity of the coating since none of the presented plated structures exhibits significantly darker areas on its surface. Furthermore, changing the plating duration does not affect the presence of aggregates at the surface of the plated structures because all structures bear gold aggregates. The local morphology of the obtained layers (Fig. 4d and Fig. 5b, d, f) is also similar in that the dark crack-like network is no longer dominating the morphology. However, none of the gold layers is fully continuous since darker contrasts corresponding to the underlying non-conductive polymer can be distinguished in all layers regardless of the plating time.

In summary, a plating time of 5 min is sufficient to obtain a stabilized layer, that is a layer with a morphology that does not evolve further when increasing the plating time, even if it presents some local discontinuities.

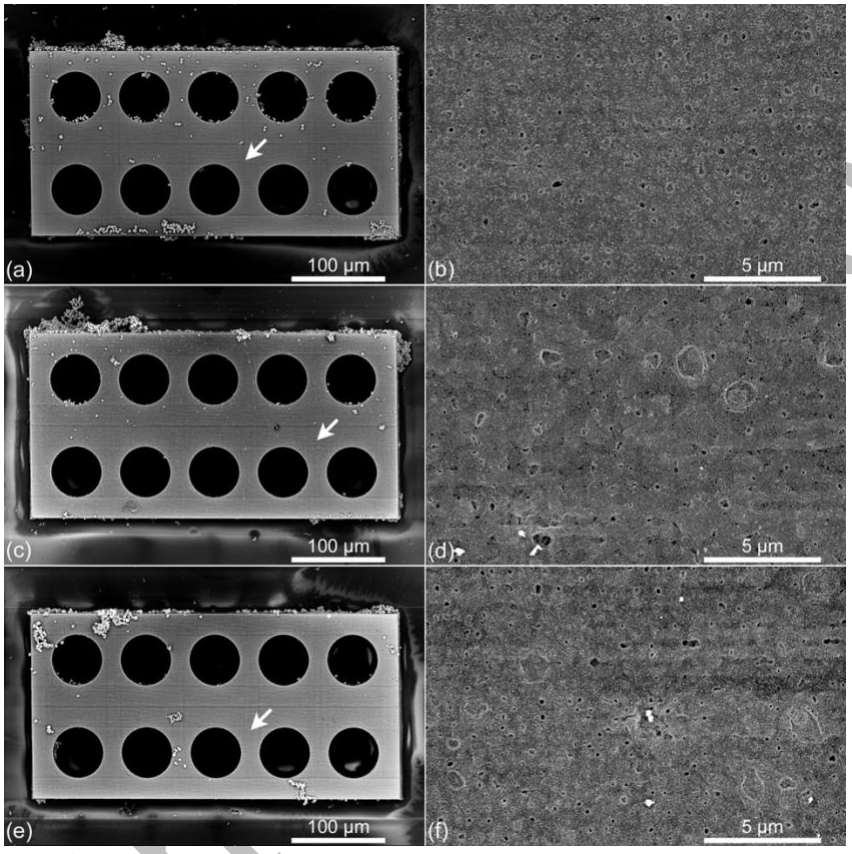

Fig. 5. BSE SEM images of the coated SZ2080 microstructures and of the corresponding gold layers for a plating step duration of (a, b) 20 min, (c, d) 10 min and (e, f) 5 min. The HCl surface modification step was performed with a solution of concentration 18.5 wt% for 2 h. The intermediate washing steps were fixed at 5 h, the Au-DMAP treatment step at 15 h, the $HAuCl_4 \bullet 3H_2O$ concentration at 0.5×10^{-2} M, and the final washing step at 2 h. The arrows in the left panels indicate the centers of the areas where the zooms of the right panels were taken.

3.3. Influence of the gold salt concentration used in the plating step

In order to study the influence of the concentration of $HAuCl_4 \bullet 3H_2O$ used in the plating step on the gold layer, the initial gold salt concentration—that is 0.5×10^{-2} M (in the order of the one chosen by Kim *et al.* [21] for polyacrylate plastics, i.e., 0.625×10^{-2} M)—was varied, thereby covering the

following concentrations: 1×10^{-2} M, 2×10^{-2} M and 3×10^{-2} M, for a plating duration of 5 min. The corresponding SEM images are reported in Fig. 6.

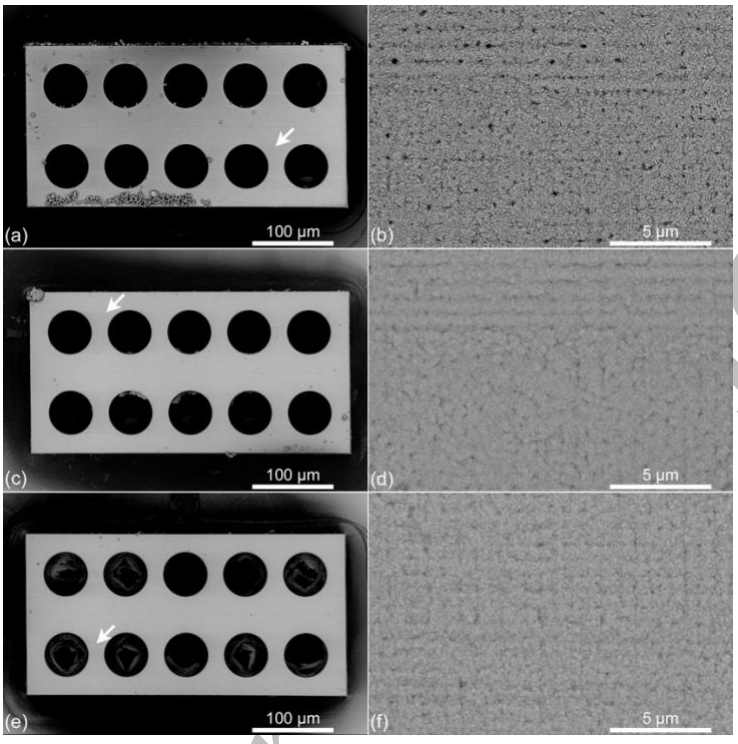

Fig. 6. BSE SEM images of the coated SZ2080 microstructures and of the corresponding gold layers for a plating step duration of 5 min with a concentration of $HAuCl_4 \bullet 3H_2O$ of (a, b) 1×10^{-2} M, (c, d) 2×10^{-2} M and (e, f) 3×10^{-2} M. The HCl surface modification step was performed with a solution of concentration 18.5 wt% for 2 h. The intermediate washing steps were fixed at 5 h, the Au-DMAP treatment step at 15 h, and the final washing step at 2 h. The arrows in the left panels indicate the centers of the areas where the zooms of the right panels were taken.

Compared to the initial concentration of 0.5×10^{-2} M (Fig. 5e), higher concentrations of 1×10^{-2} M, 2×10^{-2} M and 3×10^{-2} M (see Fig. 6a, Fig. 6c and Fig. 6e, respectively) yield gold layers exhibiting a much higher uniformity since the plated structures show much more homogeneous overall contrasts throughout the structure. Additionally, as already mentioned in Section 3.1, the amount of gold aggregates at the surface of the plated structures decreases with increasing $HAuCl_4 \bullet 3H_2O$ concentration. Some are still present for a concentration of 1×10^{-2} M but they become rare at

concentrations of 2×10^{-2} M and 3×10^{-2} M, as can also be seen on other microstructure geometries shown in Fig. 8.

The local morphology of the gold layer also evolves drastically with increasing concentration (see Fig. 6b, d, f). For a concentration of 1×10^{-2} M (Fig. 6b), the layer no longer exhibits the dark crack-like network that was characteristic of the 0.5×10^{-2} M $HAuCl_4\bullet3H_2O$ concentration. It appears that the layer has further grown, displaying gold flakes at its surface. Dark contrasts still appear but in the form of isolated holes that are well separated from each other. At $HAuCl_4\bullet3H_2O$ concentrations of 2×10^{-2} M and 3×10^{-2} M (Fig. 6d and Fig. 6f), the holes get progressively filled and the gradient in contrasts decreases. Only lighter contrasts remain, indicating that the gold layer is now fully continuous.

It is also worth mentioning here that the kinetics of the reaction is concentration dependent. From a 1×10^{-2} M $HAuCl_4\bullet3H_2O$ concentration, three stages can be clearly distinguished during the plating step: 1) the freshly made aqueous solution of $HAuCl_4\bullet3H_2O$ and $NH_2OH\bullet HCl$ is transparent and bright yellow; 2) once the seeded structure is inserted, the bright yellow color progressively disappears, and the solution becomes colorless; 3) in a final stage, the solution turns cloudy and brownish (and eventually a precipitate is formed). As the concentration increases, the duration of stage 1 decreases and that of stage 2 increases. In fact, at a 0.5×10^{-2} M $HAuCl_4\bullet3H_2O$ concentration, stage 2 is not visible, and one seems to transition directly from stage 1 to stage 3. In all cases however, 5 min are sufficient to enter stage 3. It can be hypothesized that the plating reaction occurs during stage 2 when the gold of the plating bath migrates towards the seeded structures, and that during stage 3, only the seeds that have been dispersed in the solution further react. This explains why plating times beyond 5 min do not change further the morphology of the obtained layer. Ending the plating step during stage 2 after the solution becomes colorless has been

explored, but the obtained layer morphology was varying slightly from sample to sample. As a matter of fact, estimating visually when the solution becomes fully colorless is quite user dependent. As a result, setting a plating time of 5 min, whichever the concentration, appears to yield consistent results without significantly lengthening the overall procedure.

3.5. Chemical composition

EDX spectroscopy spectra gathered with identical operating conditions on a 40 µm x 27 µm area on the coatings obtained after a 5 min plating with $HAuCl_4 \bullet 3H_2O$ concentrations of 0.5×10^{-2} M and 3×10^{-2} M are reported in Fig. 7a. For the 0.5×10^{-2} M concentration (yellow curve in Fig. 7a), the predominant peak is Au. Other peaks in the spectrum correspond to C, Si and O, that are constitutive elements of the underlying polymer. For the 3×10^{-2} M concentration (orange curve in Fig. 7a), the Au peak largely dominates the spectrum, while only a faint peak related to C appears in the rest of the spectrum. This indicates that, in both cases, gold has formed on the surface of the structure. However, in the interaction volume between the beam and the probed zone, much more gold is detected for the higher concentration than for the lower concentration. Since for the latter, the underlying polymer is also detected, this indicates that the layer obtained with the 3×10^{-2} M concentration is much thicker than the one obtained with the 0.5×10^{-2} M concentration.

EDX maps were then collected with identical operating conditions across the entire surface of the two above-mentioned samples. Fig. 7b shows the Au maps and Fig. 7c the Si maps, such that in both cases the top half corresponds to the sample plated with a 0.5×10^{-2} M $HAuCl_4 \bullet 3H_2O$ concentration and the bottom half corresponds to the sample plated with a 3×10^{-2} M $HAuCl_4 \bullet 3H_2O$ concentration. In the Au maps of Fig. 7b, the signal is generally more intense in the lower half, thereby showing that more gold is sampled by EDX when the $HAuCl_4 \bullet 3H_2O$ concentration is higher. Furthermore, in the top half corresponding to the 0.5×10^{-2} M $HAuCl_4 \bullet 3H_2O$ concentration,

the intensity is not uniform throughout the sample (one can, for example, notice that the top right corner and the aggregates between the first inter-hole are yellower than the rest), which indicates that gold is not deposited uniformly at the surface of the sample whereas it is at the surface of the sample plated with a 3×10^{-2} M $HAuCl_4\bullet3H_2O$ concentration. This is consistent with the observations made when analyzing the contrasts in the BSE SEM images in the previous sections. Additionally, contrasts linked to Si sampling are barely noticeable in the lower half of Fig. 7c in which the holes of the structures cannot be clearly distinguished, whereas both contrasts and intensities are more marked in the upper half corresponding to the sampled plated at lower concentration. This implies again, as already inferred from the spectra of Fig. 7a, that the layer obtained with the 3×10^{-2} M concentration is much thicker than the one obtained with the 0.5×10^{-2} M concentration since the underlying polymer is only detected in the latter case.

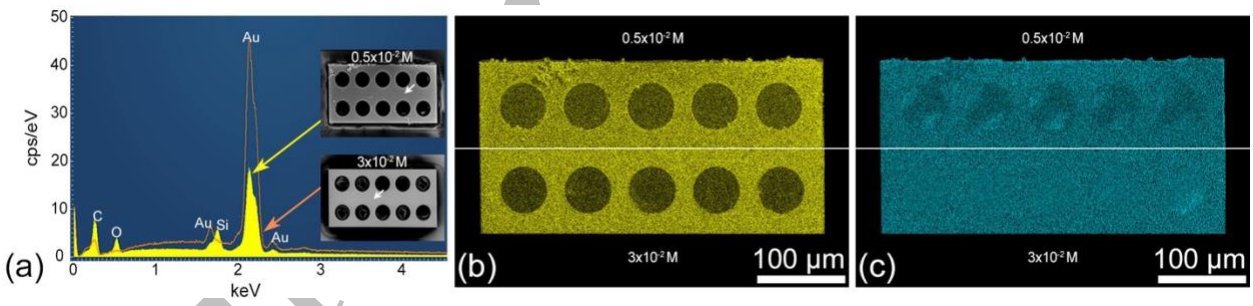

Fig. 7. (a) EDX spectroscopy spectra of the gold layers deposited on SZ2080 microstructures for a plating step duration of 5 min with a concentration of $HAuCl_4\bullet3H_2O$ of 0.5×10^{-2} M (yellow) and 3×10^{-2} M (orange). The HCl surface modification step was performed with a solution of concentration 18.5 wt% for 2 h. The intermediate washing steps were fixed at 5 h, the Au-DMAP treatment step at 15 h, and the final washing step at 2 h. The insets show the coated structures, and the arrows indicate the centers of the 40 µm x 27 µm areas where EDX data was collected. (b) Au EDX maps and (c) Si EDX map, where the top half corresponds to the 0.5×10^{-2} M concentration sample and the bottom half corresponds to the 3×10^{-2} M concentration sample.

Even though the gold layer obtained for 0.5×10^{-2} M seems to be percolating (see Fig. 5f), at least from a morphological standpoint, the layer is not conductive (see Section 3.7). Hence, only the roughness, thickness, and electrical conductivity of the coatings obtained for $HAuCl_4•3H_2O$ concentrations from 1×10^{-2} M are investigated in more details in what follows.

3.6. Gold layer roughness and thickness

The gold coatings obtained for the plating procedure using $HAuCl_4•3H_2O$ concentrations of 1×10^{-2} M, 2×10^{-2} M and 3×10^{-2} M for a plating duration of 5 min were investigated in more details. As a reminder, the HCl surface modification step was performed with a solution of concentration 18.5 wt% for 2 h. The intermediate washing steps were fixed at 5 h, the Au-DMAP treatment step at 15 h, and the final washing step at 2 h.

AFM scans were performed on the gold layers deposited on the surface of the 3D printed structures. The measurements were taken at the same location for the three cases because the structures, even after HCl treatment, still bear long-range undulations resulting from the printing process, which are specific to the selected location (see Fig. S3, and Section 4 of the Supplementary Material). The AFM scans are shown in Fig. S5, and the corresponding roughness values are reported in Table 1. At another location, where the layers were voluntarily scratched, larger AFM scans were performed so that they encompassed the scratch as well as the pristine gold layer on both sides of the scratch. The layer thickness was then obtained as the difference between the average heights of the gold layer and of the scratch area where the polymer was uncovered. The reported standard deviation corresponds to the average of the standard deviations of the heights.

Table 1. Roughness values (i.e., arithmetical mean height S_a and root mean square height S_q) and thickness of the gold layers deposited at the top surface of the SZ2080 structures for a plating step duration of 5 min with different concentrations of $HAuCl_4 \bullet 3H_2O$. The HCl surface modification step was performed with a solution of concentration 18.5 wt% for 2 h. The intermediate washing steps were fixed at 5 h, the Au-DMAP treatment step at 15 h, and the final washing step at 2 h.

$HAuCl_4 \bullet 3H_2O$ concentration	Arithmetical mean height roughness S_a (nm)	Root mean square height roughness S_q (nm)	Thickness/standard deviation (nm)
1×10^{-2} M	39	50	64/8
2×10^{-2} M	38	49	177/11
3×10^{-2} M	26	33	232/9

The roughness values from the AFM scans show that the roughness decreases first slightly when increasing the $HAuCl_4 \bullet 3H_2O$ concentration from 1×10^{-2} M to 2×10^{-2} M, and then more markedly when increasing the concentration up to 3×10^{-2} M. This is consistent with the SEM images showing the morphology of the corresponding gold layers in Fig. 6 as well as the height scans reported in Fig. S5. Indeed, as the $HAuCl_4 \bullet 3H_2O$ concentration increases, the holes initially present in the 1×10^{-2} M concentration layer get progressively filled to finally lead to a more continuous gold layer when reaching 3×10^{-2} M.

As the $HAuCl_4 \bullet 3H_2O$ concentration increases, the thickness of the layer increases as could be expected since more gold is available to nucleate and coalesce at the surface of the structure during the plating step. Hence, the layer thickness can be directly and simply controlled by tuning the concentration of $HAuCl_4 \bullet 3H_2O$ used in the plating step. As discussed in Section 3.4, beyond a 5 min plating duration, time has no more effect on the gold layer morphology and thickness because all the available gold is consumed in the first minutes of the reaction and the bath becomes

transparent, especially above 1×10^{-2} M. Trying to control the layer thickness via plating duration, i.e., by removing the structures before full completion of the reaction, would thus be too uncertain or cumbersome as the kinetics of the reaction also depends on the temperature of the room, which may not always be exactly regulated. This is in contrast with other deposition techniques, such as sputtering and ALD, in which the layer thickness can be precisely controlled by the duration of the deposition process [36,37].

3.7. Gold layer electrical conductivity

The conductivity of the gold coatings was measured with a collinear four-point probe system in which the probes are 2.6 mm apart. There exists no system, to the best of our knowledge, that can be used to conduct electrical sheet resistance measurements or resistivity measurements directly on micrometric structures (400 µm x 200 µm x 80 µm, in the present case). Hence, as detailed in Section 6 of the Supplementary Material, the measurements were instead conducted on the glass slides bearing the structures since they were submitted to the same electroless plating procedure.

With a current bias of 0.1 A, the set 20 V compliance was reached when conducting the measurements on the layer obtained with an $HAuCl_4{\bullet}3H_2O$ concentration of 0.5×10^{-2} M. The applied current was progressively decreased down to 100 nA but the system still reached compliance, indicating that the resistance between the probes was higher than 200 MΩ. It can thus be concluded that, despite displaying a seemingly percolating morphology (see Fig. 5f), the layer obtained with a 0.5×10^{-2} M concentration is not conductive.

On the other hand, the gold layers obtained with $HAuCl_4{\bullet}3H_2O$ concentrations of 1×10^{-2} M, 2×10^{-2} M and 3×10^{-2} M were found to be conductive. Their corresponding resistivities are reported in Table 2, as well as their relative resistivities when compared to bulk gold resistivity (2.44×10^{-8}

Ω.m). Increasing the $HAuCl_4 \bullet 3H_2O$ concentration appears to increase the conductivity of the layer. However, the effect of the concentration increase is stronger on the thickness evolution than it is on the resistivity, as highlighted in Fig. S8. Indeed, going from 1×10^{-2} M to 3×10^{-2} M multiplies the thickness by 3.6 whereas it only decreases the resistivity (or increases the conductivity) by 1.2.

Table 2. Resistivity of the gold layers for a plating step duration of 5 min with different concentrations of $HAuCl_4 \bullet 3H_2O$. The HCl surface modification step was performed with a solution of concentration 18.5 wt% for 2 h. The intermediate washing steps were fixed at 5 h, the Au-DMAP treatment step at 15 h, and the final washing step at 2 h.

$HAuCl_4 \bullet 3H_2O$ concentration	Resistivity (10^{-8} Ω.m)	Relative resistivity to bulk gold
1×10^{-2} M	4.63	1.90
2×10^{-2} M	4.50	1.85
3×10^{-2} M	3.72	1.53

Nevertheless, the obtained layers display very good electrical properties when compared to bulk gold since the least conductive layer is only 1.90 more resistive than bulk gold when the most conductive layer is 1.53 more resistive than bulk gold. Very similar results were obtained for copper electroless plating of plastics with resistivities between 1.1 times [38,39] and 3 times [40] that of bulk copper. Reported electrical results on gold electroless plating of plastics are however more disparate with resistivities ranging from 860 times [41] to 4,550 times [21] that of bulk gold.

3.8. Conformality of the gold coating on more complex structures

Finally, conformality of the coatings obtained with $HAuCl_4 \bullet 3H_2O$ concentrations of 1×10^{-2} M, 2×10^{-2} M and 3×10^{-2} M was demonstrated on lattice structures having different densities and bar

diameters. Double body-centered cubic lattices with overall dimensions 220 µm x 120 µm x 120 µm and 20 µm diameter bars (Fig. 8a, c, e), as well as tetrahedra with overall dimensions 110 µm x 95 µm x 90 µm and 5 µm diameter bars (Fig. 8b, d, f), all show a good conformality of the coatings on non-planar and aerated structures. As also noticed on the parallelepipedic structures, gold aggregates are nearly absent on the structures coated with 2×10^{-2} M and 3×10^{-2} M $HAuCl_4\bullet3H_2O$ concentrations (Fig. 8c-f).

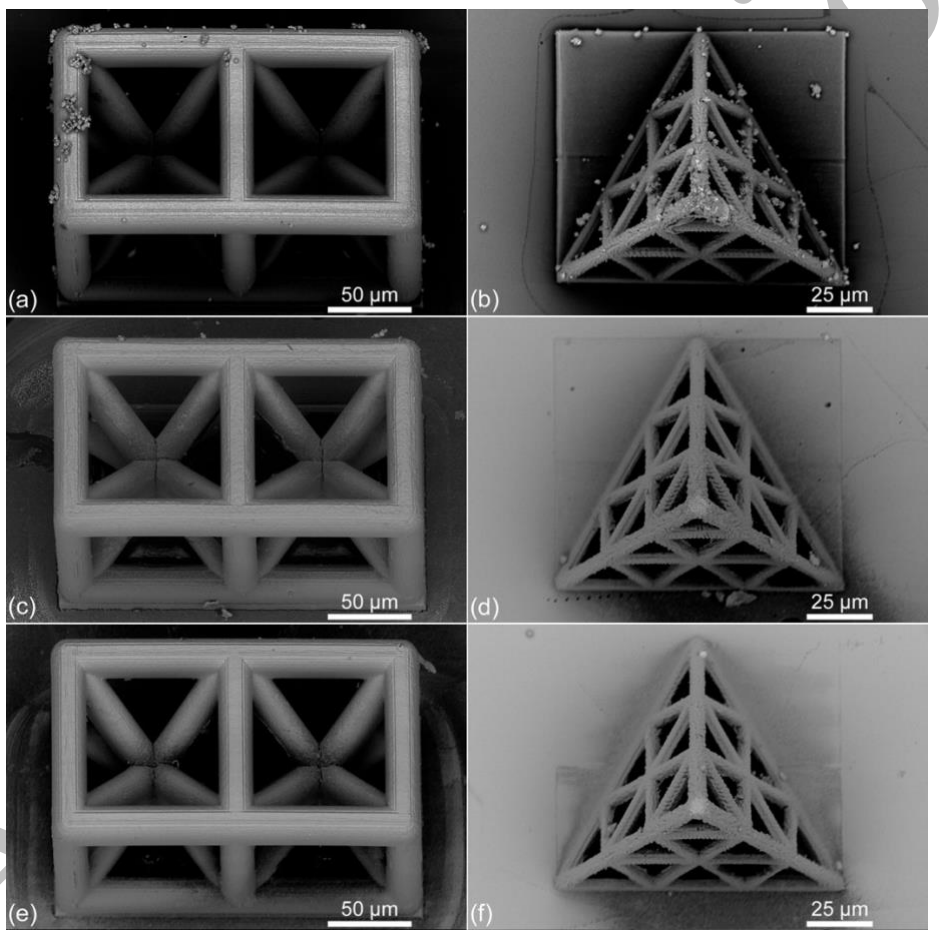

Fig. 8. BSE SEM images of coated SZ2080 3D microstructures for a plating step duration of 5 min with a concentration of $HAuCl_4\bullet3H_2O$ of (a, b) 1×10^{-2} M, (c, d) 2×10^{-2} M and (e, f) 3×10^{-2} M. The HCl surface modification step was performed with a solution of concentration 18.5 wt% for 2 h. The intermediate washing steps were fixed at 5 h, the Au-DMAP treatment step at 15 h, and the final washing step at 2 h.

4. Conclusions

A simple and efficient metallization method by electroless plating was investigated to deposit gold on the surface of hybrid organic-inorganic polymer microstructures 3D printed by TPP. The influence of the method parameters on the quality and properties of the deposited gold layer were studied. The conditions were set to be mild enough to avoid detachment or dissolution of the structures, but effective enough to yield a continuous and electrically conductive gold deposition at minimal duration and material cost.

After studying the different parameters of the electroless plating procedure, the gold plating procedure can be fixed as follows for the SZ2080 3D printed structures:

1) 2 h surface modification treatment with 18.5 wt% HCl concentration,
2) 5 h soaking in deionized H_2O,
3) 15 h Au-DMAP treatment,
4) 5 h soaking with deionized H_2O,
5) 5 min electroless plating step using 2×10^{-2} M $HAuCl_4\bullet3H_2O$,
6) 2 h soaking in deionized H_2O.

In the surface modification step, HCl concentration is the predominant parameter. A higher concentration—up to 18.5 wt%, after which the structures are no longer preserved on their substrate—leads to a better overall uniformity and continuity of the layer. Conversely, increasing the treatment time beyond 2 h does not lead to any improvement in the quality of the gold layer, and, in fact, further increases the long-range roughness present at the surface of the structures because of the printing process. In the seeding step, the concentration of the Au-DMAP solution needs to be adapted so that the surface tension of the solution front does not peel the structures off their substrate upon insertion or removal. The final morphology and properties of the obtained

gold layer are largely controlled by the $HAuCl_4 \cdot 3H_2O$ concentration in the plating bath, rather than they are by the plating duration. It appears that a 2×10^{-2} M concentration yields an overall uniform and continuous layer, with no local heterogeneities, almost no aggregates, a relatively smooth surface as well as a nearly metallic conductivity. The retained procedure is also shown to be reproducible (see Section 7 of the Supplementary Material). Finally, it leads to the deposition of a continuous gold layer on the surface of SZ2080 3D printed structures of arbitrary shapes without further refinement of the parameters, contrary to ALD for which an intensive tuning of the parameters, sometimes involving modeling, may be necessary [42].

The entire workflow of the method, with associated times, is reported in Fig. S10 of the Supplementary Material. Future investigations by the authors on the present topic include two main directions. The first concerns selectivity, so as to deposit a gold layer on the 3D printed structure but not on the substrate to which it is attached. The second aspect relates to the electrical measurements for which further developments need to be specifically conducted to handle objects of micrometric size. In a broader perspective, rendering 3D printed dielectric microstructures conductive is a topic of interest for numerous applications ranging from photonic crystals and metamaterials [43] to micro electromechanical systems [44] to complex 3D micro-electrodes [45].

CRediT authorship contribution statement

Kateryna Bretosh: Investigation, Methodology, Writing – original draft

Simon Hallais: Investigation, Methodology

Clotaire Chevalier-Cesar: Investigation

Gaël Zucchi: Supervision, Writing, Investigation – review & editing

Laurence Bodelot: Conceptualization, Project administration, Supervision, Investigation, Writing – review & editing

Declaration of Competing Interest

The authors declare that they have no known competing financial interests or personal relationships that could have appeared to influence the work reported in this paper.

Acknowledgements

This work was supported by the AID (grant number 2020 65 0055). It also benefited, through the use of the PLATINE platform, from the support of École Polytechnique fundraising – Smart environments: Nanosensors and Nanoreliability Initiative. The FEI Quanta 600 FEG SEM was acquired with the financial support of Région Ile-de-France (SESAME 2004 program), CNRS, and École Polytechnique.

References

[1] T.D. Ngo, A. Kashani, G. Imbalzano, K.T.Q. Nguyen, D. Hui, Additive manufacturing (3D printing): a review of materials, methods, applications and challenges, Compos. B Eng. 143 (2018) 172–196. https://doi.org/10.1016/j.compositesb.2018.02.012.

[2] S. Maruo, O. Nakamura, S. Kawata, Three-dimensional microfabrication with two-photon-absorbed photopolymerization, Opt. Lett. 22 (1997) 132–134. https://doi.org/10.1364/OL.22.000132.

[3] L. Jonušauskas, D. Mackevičiūtė, G. Kontenis, V. Purlys, Femtosecond lasers: the ultimate tool for high-precision 3D manufacturing, Adv. Opt. Technol.. 8 (2019) 241–251. https://doi.org/doi:10.1515/aot-2019-0012.

[4] V. Harinarayana, Y.C. Shin, Two-photon lithography for three-dimensional fabrication in micro/nanoscale regime: A comprehensive review, Opt. Laser Technol. 142 (2021) 107180. https://doi.org/https://doi.org/10.1016/j.optlastec.2021.107180.

[5] H.-B. Sun, S. Matsuo, H. Misawa, Three-dimensional photonic crystal structures achieved with two-photon-absorption photopolymerization of resin, Appl. Phys. Lett. 74 (1999) 786–788. https://doi.org/10.1063/1.123367.

[6] J. Serbin, A. Ovsianikov, B. Chichkov, Fabrication of woodpile structures by two-photon polymerization and investigation of their optical properties, Opt. Express. 12 (2004) 5221–5228. https://doi.org/10.1364/OPEX.12.005221.

[7] B. Sanchez-Padilla, A. Žukauskas, A. Aleksanyan, A. Balčytis, M. Malinauskas, S. Juodkazis, E. Brasselet, Wrinkled axicons: shaping light from cusps, Opt. Express. 24 (2016) 24075–24082. https://doi.org/10.1364/OE.24.024075.

[8] S. Rekštytė, D. Paipulas, M. Malinauskas, V. Mizeikis, Microactuation and sensing using reversible deformations of laser-written polymeric structures, Nanotechnology. 28 (2017) 124001. https://doi.org/10.1088/1361-6528/aa5d4d.

[9] L. Jonušauskas, T. Baravykas, D. Andrijec, T. Gadišauskas, V. Purlys, Stitchless support-free 3D printing of free-form micromechanical structures with feature size on-demand, Sci Rep. 9 (2019) 17533. https://doi.org/10.1038/s41598-019-54024-1.

[10] F. Klein, T. Striebel, J. Fischer, Z. Jiang, C.M. Franz, G. von Freymann, M. Wegener, M. Bastmeyer, Elastic Fully Three-dimensional Microstructure Scaffolds for Cell Force Measurements, Adv. Mater. 22 (2010) 868–871. https://doi.org/https://doi.org/10.1002/adma.200902515.

[11] V. Melissinaki, A.A. Gill, I. Ortega, M. Vamvakaki, A. Ranella, J.W. Haycock, C. Fotakis, M. Farsari, F. Claeyssens, Direct laser writing of 3D scaffolds for neural tissue engineering applications, Biofabrication. 3 (2011) 45005. https://doi.org/10.1088/1758-5082/3/4/045005.

[12] E.D. Lemma, B. Spagnolo, M. De Vittorio, F. Pisanello, Studying Cell Mechanobiology in 3D: The Two-Photon Lithography Approach, Trends Biotechnol. 37 (2019) 358–372. https://doi.org/10.1016/j.tibtech.2018.09.008.

[13] M. Suter, L. Zhang, E.C. Siringil, C. Peters, T. Luehmann, O. Ergeneman, K.E. Peyer, B.J. Nelson, C. Hierold, Superparamagnetic microrobots: fabrication by two-photon polymerization and biocompatibility, Biomed. Microdevices. 15 (2013) 997–1003. https://doi.org/10.1007/s10544-013-9791-7.

[14] F. Mayer, S. Richter, P. Hübner, T. Jabbour, M. Wegener, 3D Fluorescence-Based Security Features by 3D Laser Lithography, Adv. Mater. Technol. 2 (2017) 1700212. https://doi.org/https://doi.org/10.1002/admt.201700212.

[15] N. Takeyasu, F. Formanek, K. Chiyoda, T. Tanaka, A. Ishikawa, S. Kawata, Site-selective metal deposition on 3D micro/nanostructures fabricated by two-photon polymerization, Plasmonics: Nanoimaging, Nanofabrication, Their Appl. II. 6324 (2006) 63240W. https://doi.org/10.1117/12.681511.

[16] E. Blasco, J. Müller, P. Müller, V. Trouillet, M. Schön, T. Scherer, C. Barner-Kowollik, M. Wegener, Fabrication of Conductive 3D Gold-Containing Microstructures via Direct Laser Writing, Adv. Mater. 28 (2016) 3592–3595. https://doi.org/10.1002/adma.201506126.

[17] T. Tanaka, A. Ishikawa, S. Kawata, Two-photon-induced reduction of metal ions for fabricating three-dimensional electrically conductive metallic microstructure, Appl. Phys Lett. 88 (2006) 081107. https://doi.org/10.1063/1.2177636.

[18] C.L. Lay, C.S.L. Koh, Y.H. Lee, G.C. Phan-Quang, H.Y.F. Sim, S.X. Leong, X. Han, I.Y. Phang, X.Y. Ling, Two-Photon-Assisted Polymerization and Reduction: Emerging Formulations and Applications, ACS Appl. Mater. & Interfaces. 12 (2020) 10061–10079. https://doi.org/10.1021/acsami.9b20911.

[19] K.M. Huang, S.C. Tsai, Y.K. Lee, C.K. Yuan, Y.C. Chang, H.L. Chiu, T.T. Chung, Y.C. Liao, Selective metallic coating of 3D-printed microstructures on flexible substrates, RSC Adv. 7 (2017) 51663–51669. https://doi.org/10.1039/c7ra11171a.

[20] E.H. Waller, G. von Freymann, From photoinduced electron transfer to 3D metal microstructures via direct laser writing, Nanophotonics. 7 (2018) 1259–1277. https://doi.org/doi:10.1515/nanoph-2017-0134.

[21] S.H. Kim, J.A. Jackson, J.S. Oakdale, J.B. Forien, J.M. Lenhardt, J.H. Yoo, S.J. Shin, X. Lepró, B.D. Moran, C.M. Aracne-Ruddle, T.F. Baumann, O.S. Jones, J. Biener, A simple, highly efficient route to electroless gold plating on complex 3D printed polyacrylate plastics, Chem. Commun. 54 (2018) 10463–10466. https://doi.org/10.1039/C8CC05368E.

[22] Y. Shacham-Diamand, T. Osaka, Y. Okinaka, A. Sugiyama, V. Dubin, 30 Years of electroless plating for semiconductor and polymer micro-systems, Microelectron. Eng. 132 (2015) 35–45. https://doi.org/10.1016/j.mee.2014.09.003.

[23] A. Eder, G.H.S. Schmid, H. Mahr, C. Eisenmenger-Sittner, Aspects of thin film deposition on granulates by physical vapor deposition, Eur. Phys. J. D. 70 (2016). https://doi.org/10.1140/epjd/e2016-70435-7.

[24] P.O. Oviroh, R. Akbarzadeh, D. Pan, R.A.M. Coetzee, T.C. Jen, New development of atomic layer deposition: processes, methods and applications, Sci. Technol. Adv. Mater. 20 (2019) 465–496. https://doi.org/10.1080/14686996.2019.1599694.

[25] E.D. Goluch, K.A. Shaikh, K. Ryu, J. Chen, J. Engel, C. Liu, Microfluidic method for in-situ deposition and precision patterning of thin-film metals on curved surfaces, Appl. Phys. Lett. 85 (2004) 3629–3631. https://doi.org/10.1063/1.1808872.

[26] H. Harada, Electroless Plating: Fundamentals and Applications, J. Japan Soc. Colour Mater. 69 (1996) 60–70. https://doi.org/10.4011/shikizai1937.69.60.

[27] Y. Okinaka, M. Hoshino, Some recent topics in gold plating for electronics applications, Gold Bull. 31 (1998) 3–13. https://doi.org/10.1007/BF03215469.

[28] X. Yan, F. Meng, Y. Xie, J. Liu, Y. Ding, Direct N2H4/H2O2 fuel cells powered by nanoporous gold leaves, Sci. Rep. 2 (2012) 2–8. https://doi.org/10.1038/srep00941.

[29] S.O. Kucheyev, J.R. Hayes, J. Biener, T. Huser, C.E. Talley, A. V. Hamza, Surface-enhanced Raman scattering on nanoporous Au, Appl. Phys. Lett. 89 (2006). https://doi.org/10.1063/1.2260828.

[30] L. Zhang, X. Lang, A. Hirata, M. Chen, Wrinkled nanoporous gold films with ultrahigh surface-enhanced Raman scattering enhancement, ACS Nano. 5 (2011) 4407–4413. https://doi.org/10.1021/nn201443p.

[31] T. Jonavičius, S. Rekštytė, M. Malinauskas, Microfabrication of 3D metallic interconnects via direct laser writing and chemical metallization, Lith. J. Phys. 54 (2014) 162–169. https://doi.org/10.3952/physics.v54i3.2956.

[32] K. Terzaki, N. Vasilantonakis, A. Gaidukeviciute, C. Reinhardt, C. Fotakis, M. Vamvakaki, M. Farsari, 3D conducting nanostructures fabricated using direct laser writing, Opt. Mater Express. 1 (2011) 586–597. https://doi.org/10.1364/OME.1.000586.

[33] A. Ovsianikov, J. Viertl, B. Chichkov, M. Oubaha, B. MacCraith, I. Sakellari, A. Giakoumaki, D. Gray, M. Vamvakaki, M. Farsari, C. Fotakis, Ultra-Low Shrinkage Hybrid Photosensitive Material for Two-Photon Polymerization Microfabrication, ACS Nano. 2 (2008) 2257–2262. https://doi.org/10.1021/nn800451w.

[34] H. Topsoe, Geometric factors in four point resistivity measurement, Bulletin. 472 (1968) 63.

[35] M. Bragaglia, V. Pascale, M. Rinaldi, F. Nanni, Silver electroless plating on 3D printed resins via stereolithography: A sustainable solution, Thin Solid Films. 757 (2022) 139417. https://doi.org/https://doi.org/10.1016/j.tsf.2022.139417.

[36] P. Malinský, P. Slepička, V. Hnatowicz, V. Švorčík, Early stages of growth of gold layers sputter deposited on glass and silicon substrates, Nanoscale Res. Lett. 7 (2012) 241. https://doi.org/10.1186/1556-276X-7-241.

[37] H. Kim, H.-B.-R. Lee, W.-J. Maeng, Applications of atomic layer deposition to nanofabrication and emerging nanodevices, Thin Solid Films. 517 (2009) 2563–2580. https://doi.org/https://doi.org/10.1016/j.tsf.2008.09.007.

[38] Y.C. Liao, Z.K. Kao, Direct writing patterns for electroless plated copper thin film on plastic substrates, ACS Appl. Mater. Interfaces. 4 (2012) 5109–5113. https://doi.org/10.1021/am301654j.

[39] Y. Zhang, T. Zhang, H. Shi, Q. Liu, Y. Shi, T. Wang, Electroless Plating Cycle Process for High-Conductivity Flexible Printed Circuits, ACS Sustain. Chem. Eng. 9 (2021) 11991–12004. https://doi.org/10.1021/acssuschemeng.1c04613.

[40] Y. Zhang, T. Zhang, H. Shi, Q. Liu, T. Wang, Fabrication of flexible copper patterns by electroless plating with copper nanoparticles as seeds, Appl. Surf. Sci. 547 (2021) 149220. https://doi.org/https://doi.org/10.1016/j.apsusc.2021.149220.

[41] R. Yadav, K. Balasubramanian, Metallization of electrospun PAN nanofibers via electroless gold plating, RSC Adv. 5 (2015) 24990–24996. https://doi.org/10.1039/c5ra03531g.

[42] V. Cremers, R.L. Puurunen, J. Dendooven, Conformality in atomic layer deposition: Current status overview of analysis and modelling, Appl. Phys. Rev. 6 (2019) 021302. https://doi.org/10.1063/1.5060967.

[43] J.K. Gansel, M. Thiel, M.S. Rill, M. Decker, K. Bade, V. Saile, G. von Freymann, S. Linden, M. Wegener, Gold Helix Photonic Metamaterial as Broadband Circular Polarizer, Science 325 (2009) 1513–1515. https://doi.org/10.1126/science.1177031.

[44] T. Kan, A. Isozaki, N. Kanda, N. Nemoto, K. Konishi, H. Takahashi, M. Kuwata-Gonokami, K. Matsumoto, I. Shimoyama, Enantiomeric switching of chiral metamaterial for terahertz polarization modulation employing vertically deformable MEMS spirals, Nat. Commun. 6 (2015) 8422. https://doi.org/10.1038/ncomms9422.

[45] A. Ambrosi, J.G.S. Moo, M. Pumera, Helical 3D-Printed Metal Electrodes as Custom-Shaped 3D Platform for Electrochemical Devices, Adv. Funct. Mater. 26 (2016) 698–703. https://doi.org/https://doi.org/10.1002/adfm.201503902.